 doi:10.20944/preprints202104.0038.v1

Synthesis of ZnO Nanoparticles by using Rosmarinus officinalis Extract and their Application for Methylene bleu and Crystal violet Dyes Degradation under Sunlight irradiation

Tahani Al-Garni, Naaser A.Y. Abduh, Abdullah Al Kahtani, Ahmed Aouissi*

Department of Chemistry, King Saud University, P.O. Box 2455, Riyadh-11451, Saudi Arabia

Chemistry Department, College of Science, King Saud University, Riyadh, Saudi Arabia
* Corresponding Author. E-mail: aouissia@KSU.EDU.SA
Tel.: +966 1 4675958; Fax: +966 1 4675992.

Abstract: Zinc oxide (ZnO) nanoparticles (NPs) were synthesized using Rosmarinus officinalis leaf extract at 80 ° C (ZnO-80) and 180 ° C (ZnO-180). The biosynthesized ZnO NPs were characterized and their photocatalytic activity was evaluated for the degradation of methylene blue (MB) and crystal violet (CV) under sunlight irradiation. The results of the characterizations by XRD, TEM and SEM showed that the size of the NPs of ZnO-80 was smaller than that of ZnO-180 which exhibited flakier agglomerated spherical structures. Photocatalytic tests showed ZnO-80 which was prepared by a cheap and easy procedure compared to ZnO-180 effectively degrades MB and CV dyes under sunlight. The superior performance of ZnO-80 over ZnO-180 can be explained by the differences in their textural properties. This is because ZnO-80 has a smaller crystallite size, a specific surface area and a higher pore volume than ZnO-180. Fourier-transform infrared spectroscopy (FTIR) analyzes revealed that both samples contained an adsorbed carboxylate group (COO^-), and accordingly a mechanism was proposed for the formation of ZnO NPs that include the carboxyl group.

Keywords: dye; ZnO; NPs; leaf extract; Rosmarinus officinalis; photodegradation; methylene bleu; crystal violet

1. Introduction

The removal of organic contaminants from wastewater, and especially those resulting from dyes, remains a major concern for several countries. Indeed, environmental contamination caused by dyes leads to health problems due to their toxicity [1-5]. Dyes are organic

Preprints (www.preprints.org) | NOT PEER-REVIEWED | Posted: 2 April 2021 doi:10.20944/preprints202104.0038.v1

compounds used in various industries, such as textiles, paper, plastics, leather plastics, food, printing and pharmaceuticals, electroplating and agriculture [6-8]. It should be noted that these industries use considerable quantities of water and consequently their wastewater containing dyes in significant quantities are discharged into natural waters. Some of these dyes are toxic, mutagenic and carcinogenic [10]. Moreover, these dyes, by preventing the penetration of solar light into water, reduce photosynthetic activity and thus cause a disturbance of the aquatic equilibrium [11]. Il should be mentioned that without appropriate treatments, these dyes can remain in the natural water for a long time [12]. This is why various physical methods such as adsorption [13, 14], coagulation [15, 16], biodegradation [17, 18], and various chemical methods such as chlorination, ozonation, etc. [19] have been used to reduce the environmental effects of dyes. However, physical and biological methods do not remove pollutants; they only transform them into another phase. As for chemical methods, they have the drawback of using strong oxidants such as chlorine and ozone which are themselves pollutants. The most suitable way to eliminate this waste is their degradation by photocatalysis. In fact, dyes can be degraded in the presence of photocatalyst when irradiated with visible light due to their absorption in the visible region.

In the last decades, particular interest has been focused on heterogeneous photodegradation by metal oxides because of their wide use in organic synthesis and their environmental applications [20, 21]. Among the different metal oxides used, it has been reported that titanium dioxide (TiO_2) and zinc oxide (ZnO) are the most chemically stable and are not toxic [22-24]. This is what explains their applications in different fields [25, 26]. TiO_2 has been widely studied as a photocatalyst and found to have very good photocatalytic activity. However, its application using solar energy is strongly limited by its wide forbidden band (3.2 eV) and its low quantum efficiency [27]. As for ZnO, it is a type of semiconductor which has a wide direct band gap (3.37 eV), a large excitation binding energy (60 meV) [28]. In addition, ZnO not only has anti-fouling and antibacterial properties, but also good photocatalytic activity [29]. In addition, ZnO has been shown to exhibit high absorption efficiency over a large fraction of the solar spectrum compared to TiO_2 [30]. Taking into account these properties mentioned and the non-toxic nature, good environmental stability,

Preprints (www.preprints.org) | NOT PEER-REVIEWED | Posted: 2 April 2021 doi:10.20944/preprints202104.0038.v1

strong oxidizing power, ZnO can be considered as a suitable alternative to TiO_2 photocatalyst.

Sunlight is an abundantly available source of energy and its irradiation can be exploited to develop an economically process for the photodegradation of pollutants. In the present study, the degradation of two dyes, methylene blue (MB) and crystal violet (CV) under sunlight irradiation by ZnO NPs biosynthesized at 80^{o}C and 180^{o}C was investigated.

2. Materials and methods

2.1 Plant Materials

The healthy wild Rosmarinus leaves were collected from Abha region in southern of Saudi Arabia. Zinc nitrate hexahydrate and sodium hydroxide, methylene blue (MB), crystal violet from BHD. All the chemicals used without further purification.

2.2 Preparation of leaf extract

The collected fresh and healthy leaves of Rosmarinus were washed with deionized water, shadow dried for 2–3 weeks and then powdered using mixer grinder. For the preparation of aqueous leaf extract (ALE) solution, 10 g of powder dissolved in 100 ml of deionized water, boiled at 60 ^{o}C for 15 min to kill the pathogens in ALE solution. After cooling, ALE solution was filtered using filter paper and stored at 4 ^{o}C for further use.

2.3 Synthesis of ZnO NPs using Rosmarinus leaf extract.

ZnO NPs were prepared by adding zinc nitrate hexahydrate to aqueous leaf extract solution (ALE). Two samples were prepared; the first sample was prepared by adding 18 ml of NaOH (2M) to a solution constituted of 5g $Zn(NO_3)_2.6H_2O$ in 30 ml of the plant extract contained in an Erlenmeyer flask. The Erlenmeyer flask containing the resulting mixture was closed and then heated to 80 °C with stirring for 3 hours. The catalyst thus prepared was denoted ZnO-80. The second sample was prepared in the same way but instead of being heated in the Erlenmeyer flask, it was transferred to a Teflon lined steel autoclave and heated at 180

Preprints (www.preprints.org) | NOT PEER-REVIEWED | Posted: 2 April 2021 doi:10.20944/preprints202104.0038.v1

°C for 3 hours. The catalyst thus prepared was denoted ZnO-180. In both cases the obtained white precipitate was separated and washed several times with a solution of distilled water: ethanol (3:1). Then, it was left in the oven at 80 °C overnight and calcined in a furnace at 500 °C for 3 h. An illustrative scheme is given in Figure 1.

Figure 1. Schematic presentation of ZnO-NPs synthesis using Rosmarinus officinalis leaf extract.

2.4 Photocatalyic test

10 mg of photocatalyst and 10 ml of 10 ppm of dyes was suspended in a bottle and the mixture was stirred in the dark to evaluate adsorption–desorption equilibrium. The photodegradation was carried under sun light irradiation in a clear day of September (temperature 40 °C) at Riyadh, Longitude 46:625 Width 24:727. The resulting suspension was centrifuged at 3000 rpm for 5 minutes before measuring the absorbance using UV-Vis spectrophotometer. The photo-degradation rate of methylene blue (MB) was calculated by the following Eq. (1) [31]:

$$\text{Degradation \%} = \frac{A_0 - A_t}{A_0} \qquad (1)$$

Preprints (www.preprints.org) | NOT PEER-REVIEWED | Posted: 2 April 2021 doi:10.20944/preprints202104.0038.v1

where A_0 is the initial absorbance of MB; A_t is the absorbance of the solution after sunlight irradiation at time *t*.

2.3 Characterization of the catalysts

Infrared spectra were recorded with an infrared spectrometer GENESIS II- FTIR (4000-400 cm^{-1}) using the KBr Pellet technique. X-ray diffraction (XRD) measurements were carried out employing an Ultima IV, X-ray Rigaku difractometer using Cu-Kα radiation. UV-Vis characterization was achieved by means of double beam UV-Vis spectrophotometer (Philips 8800). Catalysts Surface morphology was analyzed by using a JSM-7600F (JEOL Ltd, Japan) Transmission electron microscopy (TEM). Thermogravimetric Analysis (TGA) were performed using a Netzsch Thermogravimetric analyzer TGA model SAT 449 F3.

The specific surface area (B.E.T), pore volume and average pore diameter of the fresh and used catalyst was measured in Micromeritics Tristar II 3020 surface area and porosity analyzer.

3. Results and discussion

3.1 Catalysts Characterization

3.1.2 FTIR

FTIR spectra of ZnO NPs synthesized at 80°C (ZnO-80) and at 180°C (ZnO-180) as well as the Rosmarinus leaf extract used for their synthesis are shown in Figure 2. The FTIR spectrum of the leaf extract showed the bands at 605, 758, 1075, 1242, 1425, 1612, 2931, and 3389 cm−1 in the region of 400 cm^{-1} to 4000 cm^{-1}. The O–H stretch band is attributed to the hydroxyl groups of phenolic compounds and N–H stretching vibration of group NH_2 [32, 33]. The peak at 2931 cm^{-1} is assigned to C-H stretching vibrations to CH_3 and CH_2 [34]. The peak at 1612 cm^{-1} is assigned to Carbonyl (–C=O) group stretching vibration, C-N stretching and COO^- antisymemetric stretching [32]. The peak at1425 cm^{-1} is assigned to C-O stretching vibration (amide) and C-C stretching from phenyl groups and carboxylate COO^- symmetric stretching [35]. The peak at 1075 is assigned to C-O stretching vibration [36, 37]. The spectrum of ZnO-80 NPs samples showed the bands at 416, 490 cm^{-1} and 1369

Preprints (www.preprints.org) | NOT PEER-REVIEWED | Posted: 2 April 2021 doi:10.20944/preprints202104.0038.v1

cm^{-1}. Similarly, the spectrum of ZnO-180 showed the bands at 420 and 492 cm^{-1} and 1383 cm^{-1}. The pair of bands observed at 416 and 490 cm^{-1} and at 420 and 492 cm^{-1} are assigned to the tensile bond of ZnO and the oxygen vacancies in ZnO respectively. These results are in agreement with those reported in the literature [38-40]. As for the peak at 1369 cm^{-1} and 1383cm-1 observed in the spectrum of ZnO-80 spectrum and ZnO-180 spectrum respectively, it is due to the symmetrical stretching of the zinc carboxylate. As the size of the NPs increases, the content of the carboxylate (COO^-) group in the samples decreased. [40].

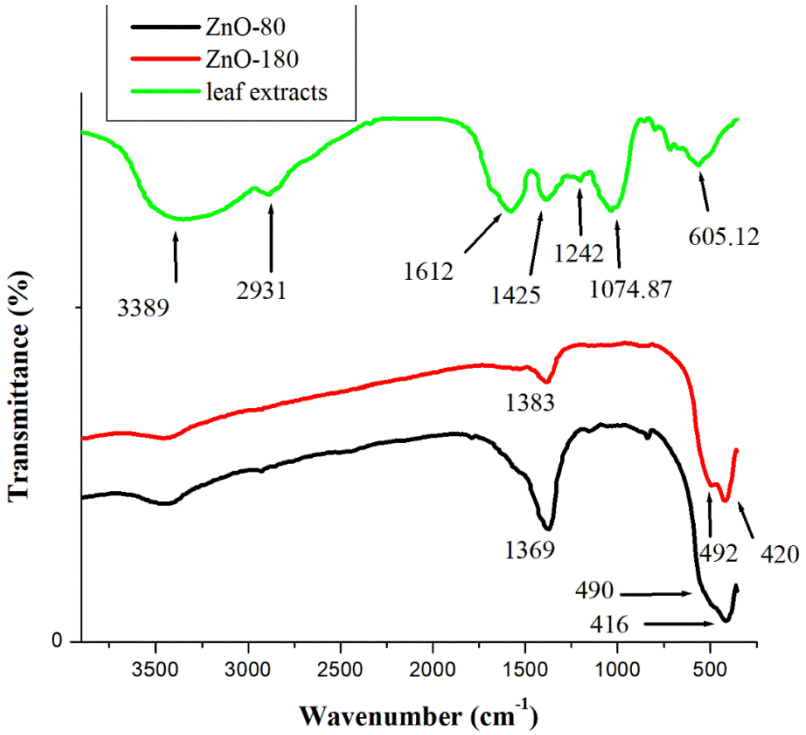

Figure 2. FTIR spectra of Rosmarinus officinalis leaf extract and ZnO NPs prepared at 80°C (ZnO-80) and 180°C (ZnO-180).

3.1.2 XRD analysis

The XRD patterns of bio-synthesized ZnO NPs from leaf extract of Rosmarinus officinalis for Zno-80 and ZnO-180 are shown in Figure 3. The sharp and narrow diffraction peaks indicate that the materials are well crystallized. The peaks found for ZnO-180 correspond to Bragg reflections with 2θ values of 31.84°, 34.48 °, 36.32 °, 47.62 °, 56.69 °, 62.95 °, 66.48

Preprints (www.preprints.org) | NOT PEER-REVIEWED | Posted: 2 April 2021 doi:10.20944/preprints202104.0038.v1

°, 68.05 °, 69.18 °. 72.59 ° and 77.07 °. The peaks found for ZnO-80 correspond to 31.74 °, 34.39 °, 36.23 °, 47.54 °, 56.60 °, 62.85 °, 67.96 °, 66.40 °, 69.09 °, 72.51 ° and 76.97 °. The X-ray diffraction patterns for both samples are in good agreement with the standard data of the hexagonal ZnO wurtzite structure (standard JCPDS card 36-1451). The reflections are attributed to the Miller-Bravais indices of (1 0 0), (0 0 2), (1 0 1), (1 0 2), (1 1 0), (1 0 3), (2 0 0), (1 1 2), (2 0 1), (0 0 4) and (2 0 2), planes of ZnO hexagonal phase structures, respectively, (standard JCPDS card 36-1451). The sharp and intense peaks indicate that the structures of the synthesized ZnO NPs were highly crystalline.

The average crystal size (D) of the particles was determined using Debye Scherer's formula, given below:

$$D = \frac{0.94\,\lambda}{\beta \cos\theta} \qquad (2)$$

where D is the crystallite size, β is the full width at half maximum, θ is the diffraction angle and λ is the wavelength of X-rays. The average crystallite size obtained for ZnO-80 and ZnO-180 was found to be 14.7 and 15.5 nm respectively.

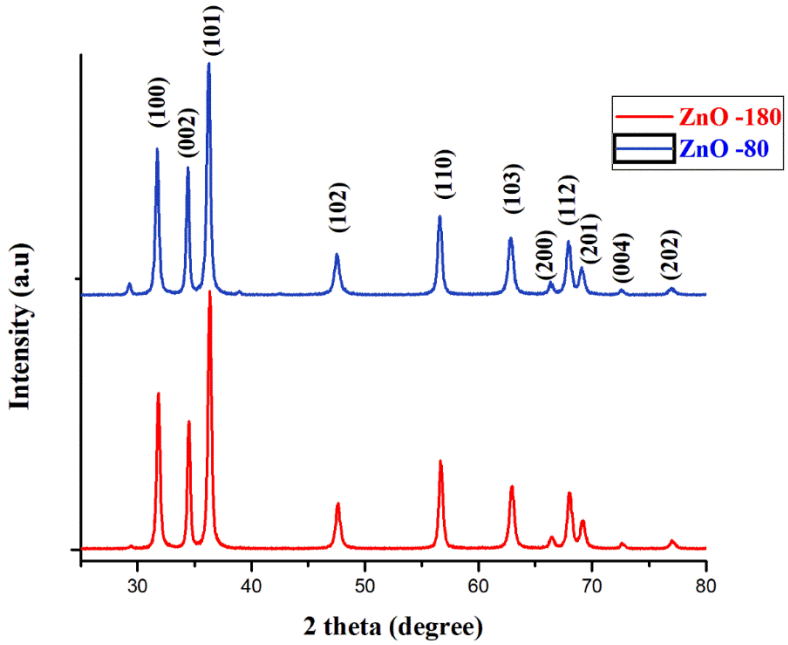

Figure 3. X-ray diffraction pattern of ZnO NPs prepared at 80°C (ZnO-80) and 180°C (ZnO-180).

Preprints (www.preprints.org) | NOT PEER-REVIEWED | Posted: 2 April 2021 doi:10.20944/preprints202104.0038.v1

3.1.3 TEM

In order to see the effect of temperature on the texture of ZnO NPs synthesized using aqueous extract of Rosmarinus officinalis leaves, characterizations by TEM were carried out. The results of the analyzes illustrated in Figure 4 show that the particles synthesized at 80°C (ZnO-80) are mainly spherical with sizes varying from 18 to 40 nm. However, some grains of larger sizes are also formed. On the other hand, NPs synthesized at 180°C (ZnO-180), they mainly have an elongated structure with sizes varying from 20 to 123nm. Some spherical particles of small sizes are also observed. The agglomerates were obtained by coalescing spherical NPs. These results are in agreement with those reported in the literature [41- 43]. Wasly et al. [41] studied the shape and size of the ZnO NPs synthesized at 100, 125, 150, 175 and 200 °C by high resolution transmission electron microscopy (HR-TEM). The results showed that the synthesis temperature affects the shape and size of ZnO NPs. Spherical shaped particles were observed at 100°C. With the increase in the reaction temperature, spherical and rod-shaped shapes of ZnO NPs were observed due to the increased growth rate. A further increase in temperature, almost all the ZnO NPs appeared in nanorod shaped clusters due to the fusion of smaller NPs and the formation of larger particles, that is, say clusters. Hassan Basri et al. [42] analyzed the structure of ZnO NPs synthesized at 28 °C and 60 °C by FESEM. NPs prepared at 28 °C clearly exhibited a mixture of spherical and rod-shaped particles, but better separated and less agglomerated compared to NPs prepared at 60 °C, which agglomerated in the shape of a flower rod. In turn, these flower-shaped particles tend to stick together to form large clusters. Dutta et al. [43] They studied the effect of temperature on the aggregation of Au NPs in the temperature range of 20 °C to 60 °C and found that the rate of aggregation increases with temperature. TEM measurements showed the formation of aggregate of Au NPs with different morphologies. The acceleration of the aggregation of NPs at higher temperatures can be explained by the decrease in the electrostatic repulsion force between NPs with increasing temperature [44-47]. It has been reported in other research work [47, 48], that the agglomerations could be due to a high surface energy of ZnO-NPs resulting from a narrow space between the NPs which generally has been observed for synthesis carried out in aqueous medium. The increased rate of aggregation with temperature is similar to ordinary chemical reactions generally observed. At higher temperatures, the NPs come together to

Preprints (www.preprints.org) | NOT PEER-REVIEWED | Posted: 2 April 2021 doi:10.20944/preprints202104.0038.v1

form nanoclusters, i.e. the average grain size increases with the annealing temperature and this was confirmed by XRD.

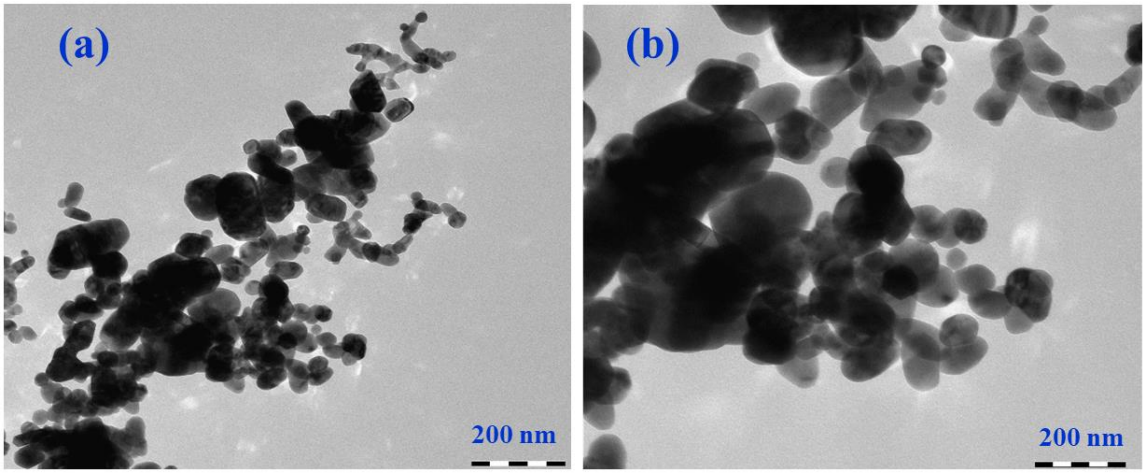

Figure 4. TEM images of: a) ZnO-80 and b) ZnO-180 prepared at 80^{o}C and 180^{o}C respectively and calcined at 500^{o}C.

3.1.4 SEM with analysis

Figure 5 shows the SEM morphology of ZnO-80 and ZnO-180 synthesized at 80 °C and 180 °C respectively. For the ZnO-80 sample, the micrograph shows individual particles with irregular morphology and an agglomerated spherical particle. On the other hand, for the ZnO-180 sample, SEM imaging shows numerous flaky agglomerated spherical structures. It should be noted that for the two samples ZnO-80 and ZnO-180, the agglomerated particles exhibited pores, probably resulting from the escape of volatile substances or gases formed during calcination. Similar observations were reported in the literature [49, 50].

Preprints (www.preprints.org) | NOT PEER-REVIEWED | Posted: 2 April 2021 doi:10.20944/preprints202104.0038.v1

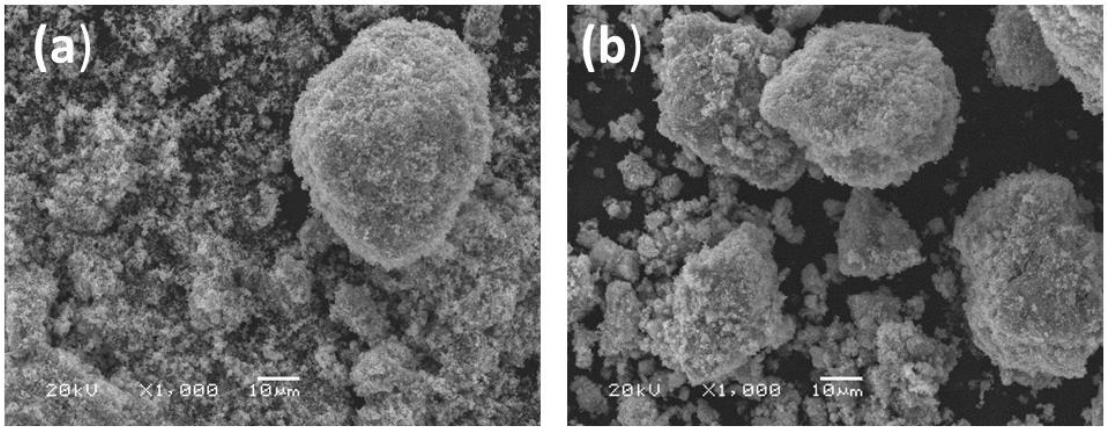

Figure 5. SEM images of: a) ZnO-80 and b) ZnO-180 prepared at 80°C and 180°C respectively and calcined at 500°C.

3.1.5 UV-visible analysis

UV-Vis spectroscopy was carried out to confirm the formation of the NPs of ZnO and to estimate the band gap value (Eg). The band gap energies of the samples were estimated using the Tauc equation :

$$(\alpha h\nu)1/2 = A(h\nu - Eg) \qquad (3)$$

where the terms *h*, ν, *α*, and *Eg* represent Planck's constant, frequency, absorption coefficient, and band gap energy, respectively. A is a proportionality constant, and *n* denotes the type of electron transition (for directly allowed transitions, $n = 1/2$). As can be seen from $(\alpha h\nu)2$ versus energy plots (Figure 6), ZnO-80 and ZnO-180 have a bandgap value of 3.30 eV and 3.26 eV respectively. The values of these band gaps are in the range of reported values of ZnO NPs [51, 52]. The bandgap of ZnO-80 material is slightly higher than that of ZnO-180. This could be due to the difference in the size of their NPs. It is well known that the variation in band gap can be due to a structural parameter and to the size of the grains. In fact, a strong correlation between absorption peak and particle size has been observed [53]. Therefore, this result indicates that the crystal particle size of ZnO-80 is smaller than that of ZnO-180, which is in agreement with those of XRD and TEM analyzes.

Preprints (www.preprints.org) | NOT PEER-REVIEWED | Posted: 2 April 2021 doi:10.20944/preprints202104.0038.v1

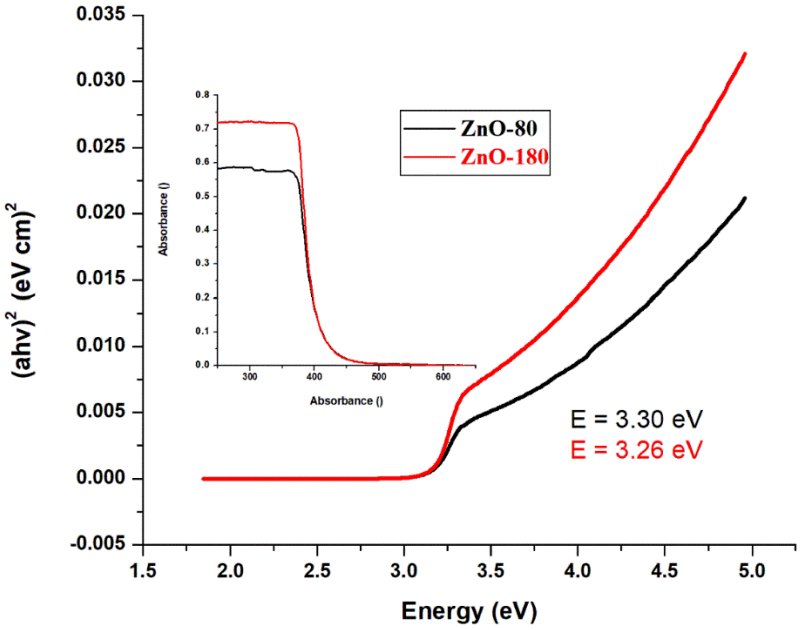

Figure 6. UV spectrum and band gab for a) ZnO-80 and b) ZnO-180 prepared at 80^{o}C and 180^{o}C respectively and calcined at 500^{o}C .

3.1.6 Thermogravimetric Analysis

TGA performed in 25 ^{o}C–1000 ^{o}C at a constant heating rate of 10 ^{o}C/minute under air atmosphere. The thermograms of both metal oxide NPs are shown in Figure 7. As can be seen, the thermogravimetric (TG) curve for both samples shows three stages of weight loss. The first stage indicates a weight loss of 1.4% and 1.3% for ZnO-80 and ZnO-180 respectively was observed at around 140 °C due to water evaporation. A second weight loss of 1.7% and 1.2% for ZnO-80 and ZnO-180 respectively appeared while temperature increases at 140–260 °C that could be attributed to the decomposition of the bio entities from the extract capped on the synthesized zinc oxide NPs. This thermal decomposition can be yet another confirmation for the presence of phytoconstituents that are functionalized on the NPs. Similar results of thermal decomposition of phytochemicals coated on the NPs have been reported [54]. A third weight loss of 5.9 % and 1.9% respectively appeared while temperature increases at 260–900°C which, probably was due to the thermal degradation of less volatile aromatic compounds [55]. It should be noted that beyond 220^{o}C the weight loss for ZnO-180 becomes greater than that observed for ZnO-80. This is consistent with the

Preprints (www.preprints.org) | NOT PEER-REVIEWED | Posted: 2 April 2021 doi:10.20944/preprints202104.0038.v1

results of SEM which shows that ZnO-180 exhibits more agglomerations which may be organic compounds coating the ZnO NPs.

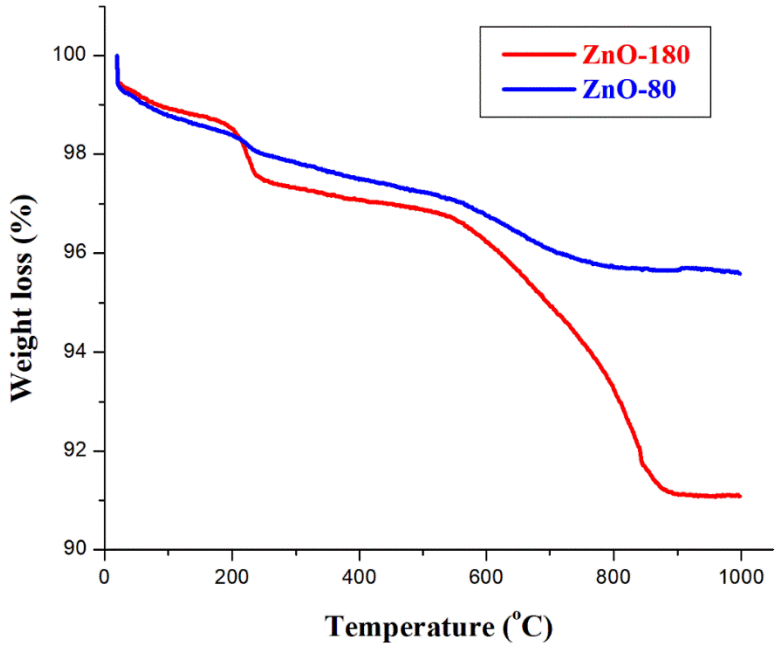

Figure 7. Thermograph of: a) ZnO-80 and b) ZnO-180 prepared at 80°C and 180°C respectively and calcined at 500°C.

Mechanism for the formation of ZnO

To establish a possible mechanism for the formation of ZnO NPs involving one of the substances present in the plant extract, it is first necessary to verify the formation of the NPs after addition of the extract. To do this, the ZnO-80 particles formed after the action of the substance but before calcination were analyzed by UV-Visible spectroscopy. By way of comparison, the characterization of the ZnO-80 particles after calcination was also carried out. The analysis was performed under aqueous conditions in the wavelength range from 250 nm to 550 nm and the results are presented in Figure 8. The absorption peaks observed at 371 and 382 nm for Zno-80 before and after calcination respectively confirms the formation of ZnO NPs. Similar results of absorption band were also observed by various researchers [56-58]. The absorption peaks observed at 371 and 382 nm are due to the

Preprints (www.preprints.org) | NOT PEER-REVIEWED | Posted: 2 April 2021 doi:10.20944/preprints202104.0038.v1

intrinsic band gap of Zn–O absorption. As for the substance probably involved in the synthesis of ZnO-80 NPs, the results of FTIR (Figure 2), showed that carboxylate species remained adsorbed on the NPs even after calcination. It is therefore probable that these species are involved in the formation of NPs. It should be noted that various leaf extracts contain substances which can act as reducing and capping agent, thus preventing aggregation of NPs. Indeed, it has been observed that the action of certain biological compounds leads to the reduction of Zn^{2+} to ZnO NPs [59]. It has also been observed that proteins and functional groups (carboxylates) are involved in the reduction of gold NPs [60]. On the other hand, it has been shown that when a zinc oxide powder is dispersed in distilled water in the pH range 7-9, it is in equilibrium with various species in aqueous solution and that is the species Zn^{2+} and $Zn(OH)^{+}$ which are the predominant [61]. It is therefore probable that the formation of ZnO NPs goes through the formation of $Zn(OH)^{+}$. Based on the above results, a mechanism (Figure 9) has been proposed.

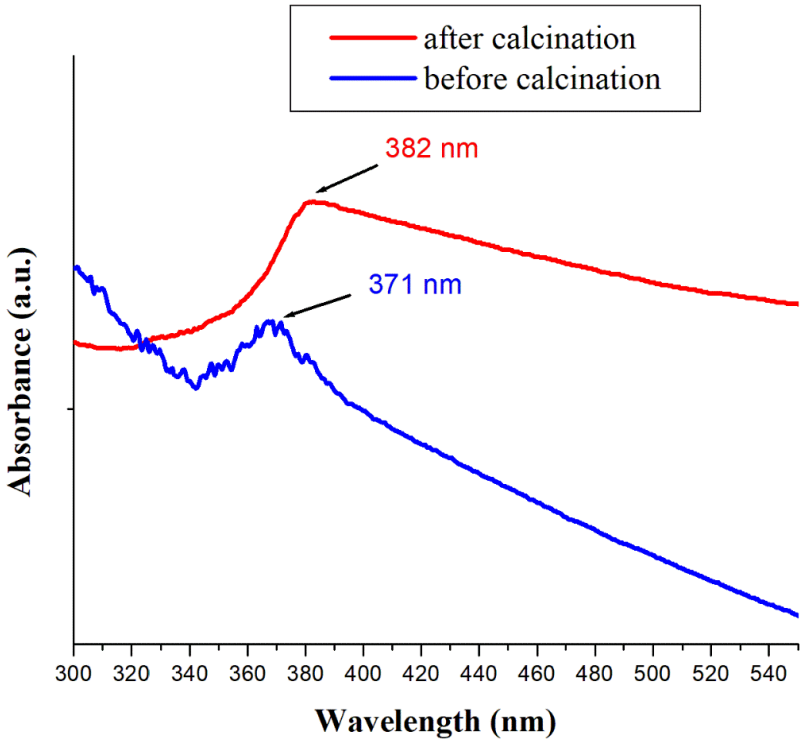

Figure 8. UV spectrum of ZnO-80: a) before calcination and b) after calcination

Preprints (www.preprints.org) | NOT PEER-REVIEWED | Posted: 2 April 2021 doi:10.20944/preprints202104.0038.v1

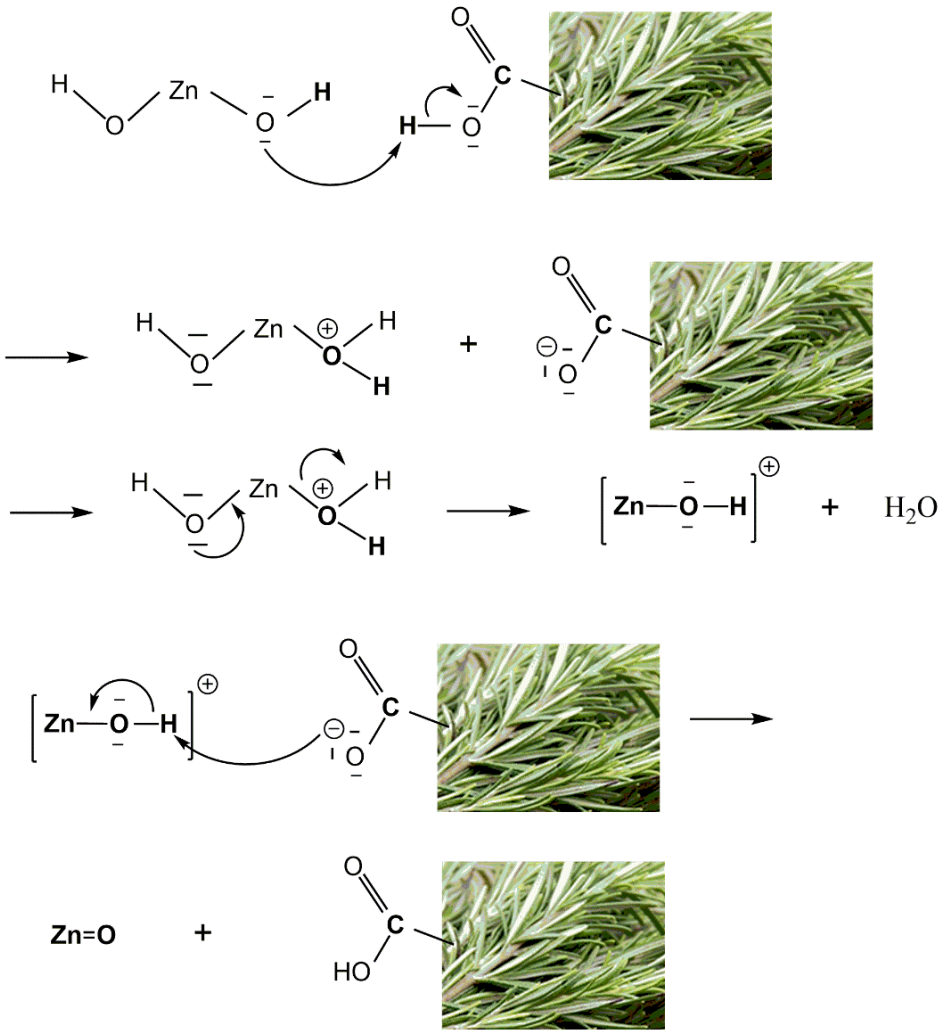

Figure 9. Possible reaction mechanism for the formation of ZnO NPs in presence of carboxyl group (–COOH) of Rosmarinus officinalis leaf extract.

3.2 Photocatalytic activity

The photocatalytic activities of the synthesized ZnO NPs were evaluated via the photodegradation of methylene blue (MB) and CV under sunlight irradiation. Prior to illumination, 10mg photocatalyst was added to the dye aqueous solution (10 mL, 10ppm). The solution was stirred in the dark for 20 minutes in order to achieve absorption-desorption equilibrium, then the photocatalytic reaction was started. The photocatalyst will then be exposed to the sunlight for the desired time at 40°C. Figure 10 shows the UV–Vis absorption spectra of MB and CV absorbance with respect to time for ZnO-80 and ZnO-180. The

Preprints (www.preprints.org) | NOT PEER-REVIEWED | Posted: 2 April 2021 doi:10.20944/preprints202104.0038.v1

aqueous solution of the MB molecules exhibits two peaks, one at 664 and the other at 615 nm, which correspond respectively to monomers and dimers. [62]. Upon irradiation, the peak at 664nm has a progressively blue shift to shorter wavelength (Figure 10 (a)) because of hypsochromic effect [63, 64]. In the presence of ZnO-80 the absorbance of MB decreased sharply after 30 min. Initially, the absorption peak at 664 nm was much larger than the absorption peak at 615 nm which gives a big difference between their intensities. After 30 min, this difference is attenuated, thus indicating that the rate of degradation of the monomers is much higher than that of the dimers [65]. In addition to the decrease in the intensities of the two peaks, a slight shift towards the blue of the bands located at 664 nm also observed. This is caused by the N-demethylated degradation concomitant with the degradation of phenothiazine [66].

The influence of the irradiation time on the discoloration of the CV (Figure 10 (b)) was followed by the characteristic peak at 590 nm, corresponding to the conjugated triphenylmethane chromophore. The decrease in absorbance at 590 nm with irradiation is due to the degradation of the chromophore responsible for the characteristic color of the CV. The hypochromic shift of the peak at 590 nm of the chromophore at about 575 nm indicates an N-dimethylation reaction [67] leading to NO_3^- ions [68, 69].

Preprints (www.preprints.org) | NOT PEER-REVIEWED | Posted: 2 April 2021 doi:10.20944/preprints202104.0038.v1

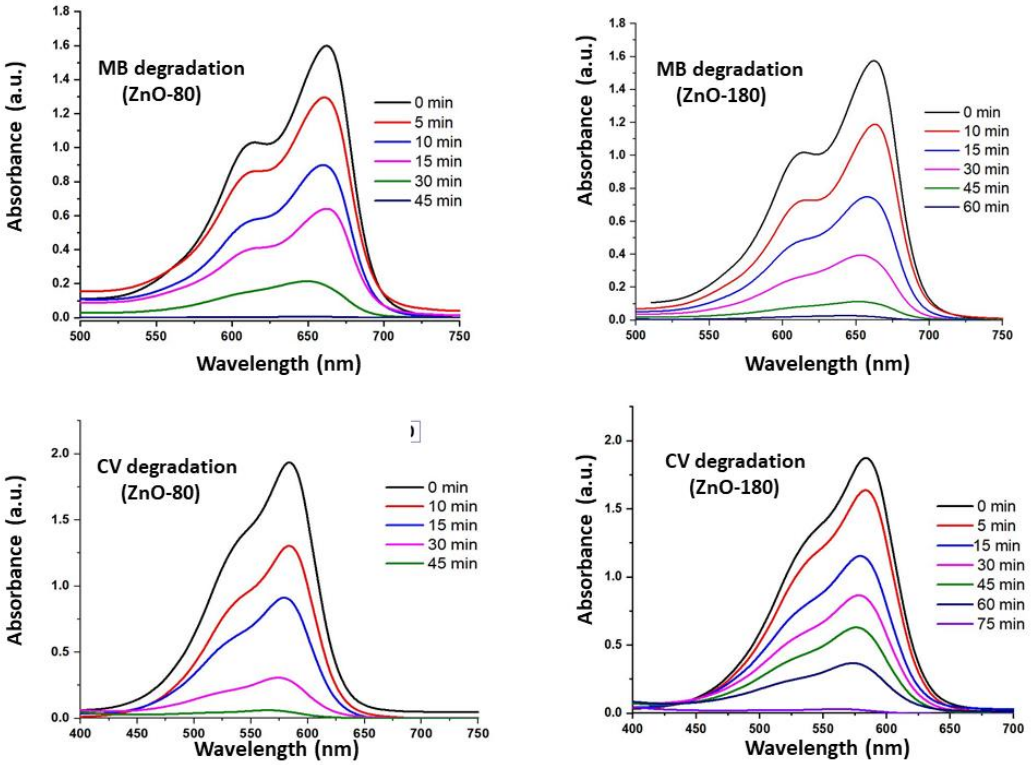

Figure 10. UV–Vis absorption spectra of degradation of MB and CV by ZnO-80 and ZnO-180 under sunlight irradiation. Reaction **c**onditions: Dye concentration 10 mg of photocatalyst and 10 ml of 10 ppm of dyes.

Figure 11 shows the decreasing concentration of MB and CV with respect to time for ZnO-80 and ZnO-180. As shown in Figure 9(a) MB was degraded completely after irradiating 45min and 60 min by ZnO-80 and ZnO-180, respectively. Whereas, the complete degradation of CV takes 60 and 75 min for ZnO -80 and ZnO-180 respectively. The higher MB and CV degradation rate over ZnO-80 proves its better performance compared to ZnO-180. These results are consistent with the texture properties of the prepared ZnO-80 and ZnO-180 photocatalysts (Table 1). It can be seen that ZnO-80 presents lower crystallite size, higher surface area and higher pore volume than ZnO-180.

Preprints (www.preprints.org) | NOT PEER-REVIEWED | Posted: 2 April 2021 doi:10.20944/preprints202104.0038.v1

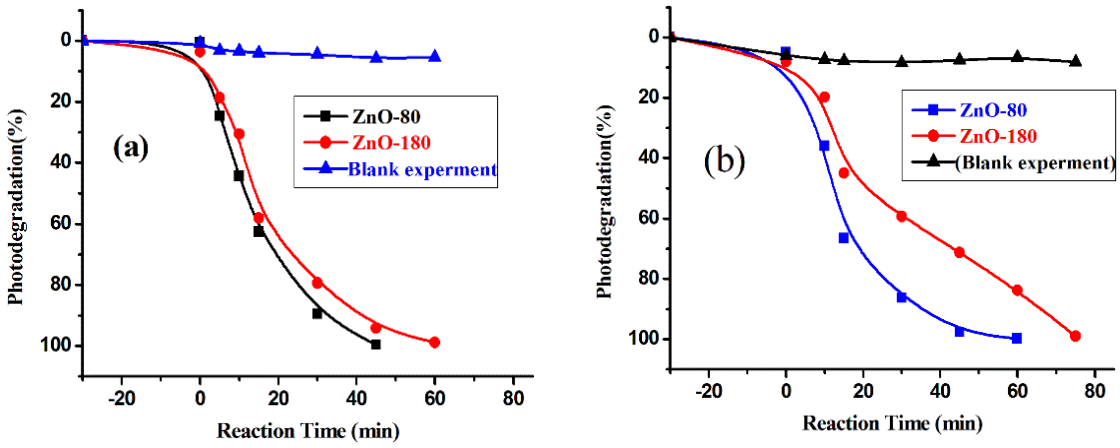

Figure 11. Effect of ZnO-80 and ZnO-180 on the photocatalytic degradation of (a) MB, (b) CV under sunlight irradiation**.** Reaction conditions: Dye concentration 10 mg of photocatalyst and 10 ml of 10 ppm of dyes

Table 1. Texture properties of the ZnO-80 and ZnO-180 metal oxide NPs.

Physical properties	ZnO-80	ZnO-180
BET Surface Area (m^2/g)	11.9958	8.6474
Pore Volume (cm^3/g)	0.236241	0.121089
Total Area in Pore (m^2/g)	7.409	5.137
Crystallite size (nm)	14.7	15.5
Pore Size (Å)	787.7445	560.1170

3.1. Reusability

In order to examine the reusability of the biosynthesized ZnO-80 and ZnO-180 photocatalysts, we tested them after use to see the stability of their photocatalytic activity. Both solids were tested under the same conditions as those in which they gave complete degradation of MB and CV, ie 100%. The results obtained (Table 2) show that ZnO-80 degrades MB by 96.7% while ZnO-180 degrades it by 93.8%. As for the discoloration of the CV, the results obtained show that the two samples, ZnO-80 and ZnO-180, discolored it to 95.1%. A slight decrease in activity therefore occurred. This is expected because a decrease in photocatalytic activity after reuse of the catalyst has been observed by many researchers [70, 71]. This slight decrease in degradation is acceptable and allows reuse of these catalysts.

Preprints (www.preprints.org) | NOT PEER-REVIEWED | Posted: 2 April 2021 doi:10.20944/preprints202104.0038.v1

Table .2 Reusability of ZnO-80 and ZnO-180 photocatalysts for the degradation of MB and CV dyes. Reaction conditions: Dye concentration 10 mg of photocatalyst and 10 ml of 10 ppm of dyes**.**

Dye	ZnO-80		ZnO-180	
	Fresh	Used	Fresh	Used
MB	100	96.7	100	93.8
CV	100	95.1	100	95.1

4. Conclusion

In the present study, the degradation of methylene blue and crystal violet dyes by ZnO NPs under sunlight irradiation was investigated. ZnO NPs were synthesized using Rosmarinus officinalis leaf extract at 80 ° C (ZnO-80) and 180 ° C (ZnO-180).

The FTIR spectra of the synthesized bio ZnO NPs showed the presence of the carboxylate group (COO^-) adsorbed on the NPs of the two samples. It is therefore probable that these species are involved in the formation of NPs. Based on these results, a mechanism has been proposed. The XRD, TEM and SEM results showed that the synthesis temperature affects the shape and size of ZnO NPs. A lower temperature leads to the production of smaller, spherical shaped and less agglomerated particles.

Photocatalytic tests revealed that ZnO-80 NPs were more efficient in photo-degradation of MB and CV dyes compared to ZnO-180. The high activity of ZnO-80 was due to better physicochemical properties compared to ZnO-180.

ZnO-80 which was prepared by a cheap and easy procedure compared to ZnO-180, which was prepared by usual method using autoclave and high temperature, effectively degrades MB and CV dyes under sunlight.

Photo-degradation of dyes under sunlight as an abundantly available energy source by ZnO, prepared by a simple method, can be exploited to develop an environmentally friendly and economical process.

Author Contributions: Tahani Al-Garni provided materials and performed characterizations, Naaser A.Y. Abduh performed the experiments and analyzed the experimental data, Abdullah Al Kahtani provided materials and funding, Ahmed Aouissi designed and wrote the article. All authors have read and accepted the published version of the manuscript.

Acknowledgements: The authors extended their appreciation to the Deanship of Scientific Research at King Saud University: [Grant Number RG-1441-507].

Conflicts of Interest: The authors declare no conflicts of interest.

References

1. Amini, M.; Ashrafi, M. Photocatalytic degradation of some organic dyes under solar light irradiation using TiO2 and ZnO NPs. *Nanochemistry Research* **2016**, *1*, 79-86.
2. Muhd Julkapli, N.; Bagheri, S.; Bee Abd Hamid, S. Recent advances in heterogeneous photocatalytic decolorization of synthetic dyes. *The Scientific World Journal* **2014**, *2014*.
3. Bremner, D.H.; Molina, R.; Martínez, F.; Melero, J.A.; Segura, Y. Degradation of phenolic aqueous solutions by high frequency sono-Fenton systems (US–Fe2O3/SBA-15–H2O2). *Applied Catalysis B: Environmental* **2009**, *90*, 380-388.
4. Amini, M.; Pourbadiei, B.; Ruberu, T.P.A.; Woo, L.K. Catalytic activity of MnO x/WO 3 NPs: synthesis, structure characterization and oxidative degradation of methylene blue. *New journal of chemistry* **2014**, *38*, 1250-1255.
5. Mani, S.; Bharagava, R.N. Exposure to crystal violet, its toxic, genotoxic and carcinogenic effects on environment and its degradation and detoxification for environmental safety. *Reviews of Environmental Contamination and Toxicology Volume 237* **2016**, 71-104.
6. El Khomri, M.; El Messaoudi, N.; Dbik, A.; Bentahar, S.; Lacherai, A. Efficient adsorbent derived from Argania Spinosa for the adsorption of cationic dye: Kinetics, mechanism, isotherm and thermodynamic study. *Surfaces and Interfaces* **2020**, *20*, 100601.
7. Ishaq, M.; Javed, F.; Amad, I.; Ullah, H.; Hadi, F.; Sultan, S. Adsorption of crystal violet dye from aqueous solutions onto low-cost untreated and NaOH treated almond shell. *Iranian Journal of Chemistry and Chemical Engineering (IJCCE)* **2016**, *35*, 97-106.

8. Ali, N.; Bilal, M.; Khan, A.; Ali, F.; Iqbal, H.M. Effective exploitation of anionic, nonionic, and nanoparticle-stabilized surfactant foams for petroleum hydrocarbon contaminated soil remediation. *Science of the Total Environment* **2020**, *704*, 135391.
9. Ahmad, I.; Khan, S.B.; Kamal, T.; Asiri, A.M. Visible light activated degradation of organic pollutants using zinc–iron selenide. *Journal of Molecular Liquids* **2017**, *229*, 429-435.
10. Fayoud, N.; Younssi, S.A.; Tahiri, S.; Albizane, A. Etude cinétique et thermodynamique de l'adsorption de bleu de méthylène sur les cendres de bois (Kinetic and thermodynamic study of the adsorption of methylene blue on wood ashes). *J. Mater. Environ. Sci* **2015**, *6*, 3295-3306.
11. Shakoor, S.; Nasar, A. Removal of methylene blue dye from artificially contaminated water using citrus limetta peel waste as a very low cost adsorbent. *Journal of the Taiwan Institute of Chemical Engineers* **2016**, *66*, 154-163.
12. Fazli, M.M.; Mesdaghinia, A.; Naddafi, K.; Nasseri, S.; Yunesian, M.; Assadi, M.M.; Rezaie, S.; Hamzehei, H. Optimization of reactive blue 19 decolorization by ganoderma sp. using response surface methodology. *Journal of Environmental Health Science & Engineering* **2010**, *7*, 35-42.
13. Hussain, S.; Ullah, Z.; Gul, S.; Khattak, R.; Kazmi, N.; Rehman, F.; Khan, S.; Ahmad, K.; Imad, M.; Khan, A. Adsorption characteristics of magnesium-modified bentonite clay with respect to acid blue 129 in aqueous media. *Polish Journal of Environmental Studies* **2016**, *25*, 1947-1953.
14. Wahid, F.; Mohammadzai, I.U.; Khan, A.; Shah, Z.; Hassan, W.; Ali, N. Removal of toxic metals with activated carbon prepared from Salvadora persica. *Arabian Journal of Chemistry* **2017**, *10*, S2205-S2212.
15. Klingenberg, M.; Becker, J.; Eberth, S.; Kube, D.; Wilting, J. The NADPH oxidase inhibitor imipramine-blue in the treatment of Burkitt lymphoma. *Molecular cancer therapeutics* **2014**, *13*, 833-841.
16. Zargar, B.; Parham, H.; Hatamie, A. Fast removal and recovery of amaranth by modified iron oxide magnetic NPs. *Chemosphere* **2009**, *76*, 554-557.
17. Xu, A.; Li, X.; Ye, S.; Yin, G.; Zeng, Q. Catalyzed oxidative degradation of methylene blue by in situ generated cobalt (II)-bicarbonate complexes with hydrogen peroxide. *Applied Catalysis B: Environmental* **2011**, *102*, 37-43.

18. Anjaneyulu, Y.; Chary, N.S.; Raj, D.S.S. Decolourization of industrial effluents–available methods and emerging technologies–a review. *Reviews in Environmental Science and Bio/Technology* **2005**, *4*, 245-273.
19. Hernández-Ramírez, A.; Medina-Ramírez, I. *Photocatalytic semiconductors*; Springer: 2016.
20. Shinde, S.; Shinde, P.; Bhosale, C.; Rajpure, K. Zinc oxide mediated heterogeneous photocatalytic degradation of organic species under solar radiation. *Journal of Photochemistry and Photobiology B: Biology* **2011**, *104*, 425-433.
21. Chang, X.; Li, Z.; Zhai, X.; Sun, S.; Gu, D.; Dong, L.; Yin, Y.; Zhu, Y. Efficient synthesis of sunlight-driven ZnO-based heterogeneous photocatalysts. *Materials & Design* **2016**, *98*, 324-332.
22. Kou, J.; Lu, C.; Wang, J.; Chen, Y.; Xu, Z.; Varma, R.S. Selectivity enhancement in heterogeneous photocatalytic transformations. *Chemical reviews* **2017**, *117*, 1445-1514.
23. Qu, X.; Alvarez, P.J.; Li, Q. Applications of nanotechnology in water and wastewater treatment. *Water research* **2013**, *47*, 3931-3946.
24. Bao, J.; Zimmler, M.A.; Capasso, F.; Wang, X.; Ren, Z. Broadband ZnO single-nanowire light-emitting diode. *Nano letters* **2006**, *6*, 1719-1722.
25. Mahadik, M.; Shinde, S.; Kumbhar, S.; Pathan, H.; Rajpure, K.; Bhosale, C. Enhanced photocatalytic activity of sprayed Au doped ferric oxide thin films for salicylic acid degradation in aqueous medium. *Journal of Photochemistry and Photobiology B: Biology* **2015**, *142*, 43-50.
26. Wang, A.-n.; Teng, Y.; Hu, X.-f.; Wu, L.-h.; Huang, Y.-j.; Luo, Y.-m.; Christie, P. Diphenylarsinic acid contaminated soil remediation by titanium dioxide (P25) photocatalysis: Degradation pathway, optimization of operating parameters and effects of soil properties. *Science of the Total Environment* **2016**, *541*, 348-355.
27. Choi, K.; Kang, T.; Oh, S.-G. Preparation of disk shaped ZnO particles using surfactant and their PL properties. *Materials Letters* **2012**, *75*, 240-243.
28. Al-Fori, M.; Dobretsov, S.; Myint, M.T.Z.; Dutta, J. Antifouling properties of zinc oxide nanorod coatings. *Biofouling* **2014**, *30*, 871-882.
29. Yogendra, K.; Naik, S.; Mahadevan, K.; Madhusudhana, N. A comparative study of photocatalytic activities of two different synthesized ZnO composites against Coralene Red F3BS dye in presence of natural solar light. *International Journal of Environmental Sciences and Research* **2011**, *1*, 11-15.

30. Zhang, X.; Zhou, G.; Zhang, H.; Wu, C.; Song, H. Characterization and activity of visible light–driven TiO 2 photocatalysts co-doped with nitrogen and lanthanum. *Transition Metal Chemistry* **2011**, *36*, 217-222.
31. Ahmed, S.; Saifullah; Ahmad, M.; Swami, B.L.; Ikram, S. Green synthesis of silver NPs using Azadirachta indica aqueous leaf extract. *Journal of radiation research and applied sciences* **2016**, *9*, 1-7.
32. Lateef, A.; Akande, M.A.; Ojo, S.A.; Folarin, B.I.; Gueguim-Kana, E.B.; Beukes, L.S. Paper wasp nest-mediated biosynthesis of silver NPs for antimicrobial, catalytic, anticoagulant, and thrombolytic applications. *3 Biotech* **2016**, *6*, 1-10.
33. Goudarzi, M.; Mir, N.; Mousavi-Kamazani, M.; Bagheri, S.; Salavati-Niasari, M. Biosynthesis and characterization of silver NPs prepared from two novel natural precursors by facile thermal decomposition methods. *Scientific reports* **2016**, *6*, 1-13.
34. Szymanska-Chargot, M.; Zdunek, A. Use of FT-IR spectra and PCA to the bulk characterization of cell wall residues of fruits and vegetables along a fraction process. *Food biophysics* **2013**, *8*, 29-42.
35. Mohammad, G.R.K.S.; Tabrizi, M.H.; Ardalan, T.; Yadamani, S.; Safavi, E. Green synthesis of zinc oxide NPs and evaluation of anti-angiogenesis, anti-inflammatory and cytotoxicity properties. *Journal of biosciences* **2019**, *44*, 1-9.
36. Khatami, M.; Mehnipor, R.; Poor, M.H.S.; Jouzani, G.S. Facile biosynthesis of silver NPs using Descurainia sophia and evaluation of their antibacterial and antifungal properties. *Journal of Cluster Science* **2016**, *27*, 1601-1612.
37. Sharma, S.; Kumar, S.; Bulchandini, B.; Taneja, S.; Banyal, S. Green synthesis of silver NPs and their antimicrobial activity against gram positive and gram negative bacteria. *Int. J. Biotechnol. Bioeng. Res* **2013**, *4*, 711-714.
38. Rehman, H.; Ali, Z.; Hussain, M.; Gilani, S.; Shahzady, T.; Zahra, A.; Hussain, S.; Hussain, H.; Hussain, I.; Farooq, M. Synthesis and characterization of ZnO NPs and their use as an adsorbent for the arsenic removal from drinking water. *Digest Journal of Nanomaterials and Biostructures* **2019**, *14*, 1033-1040.
39. Xiong, G.; Pal, U.; Serrano, J.; Ucer, K.; Williams, R. Photoluminesence and FTIR study of ZnO NPs: the impurity and defect perspective. *physica status solidi c* **2006**, *3*, 3577-3581.
40. Wasly, H.; Abd El-Sadek, M.; Henini, M. Influence of reaction time and synthesis temperature on the physical properties of ZnO NPs synthesized by the hydrothermal method. *Applied Physics A* **2018**, *124*, 76.

41. Hassan Basri, H.; Talib, R.A.; Sukor, R.; Othman, S.H.; Ariffin, H. Effect of synthesis temperature on the size of ZnO NPs derived from pineapple peel extract and antibacterial activity of ZnO–starch nanocomposite films. *Nanomaterials* **2020**, *10*, 1061.
42. Dutta, A.; Paul, A.; Chattopadhyay, A. The effect of temperature on the aggregation kinetics of partially bare gold NPs. *RSC advances* **2016**, *6*, 82138-82149.
43. Chen, Y.; Huang, Y.; Li, K. Temperature effect on the aggregation kinetics of CeO2 NPs in monovalent and divalent electrolytes. *J. Environ. Anal. Toxicol* **2012**, *2*, 158-162.
44. Li, K.; Zhang, W.; Huang, Y.; Chen, Y. Aggregation kinetics of CeO 2 NPs in KCl and CaCl 2 solutions: measurements and modeling. *Journal of Nanoparticle Research* **2011**, *13*, 6483-6491.
45. Li, K.; Chen, Y. Effect of natural organic matter on the aggregation kinetics of CeO2 NPs in KCl and CaCl2 solutions: measurements and modeling. *Journal of hazardous materials* **2012**, *209*, 264-270.
46. Salam, H.A.; Sivaraj, R.; Venckatesh, R. Green synthesis and characterization of zinc oxide NPs from Ocimum basilicum L. var. purpurascens Benth.-Lamiaceae leaf extract. *Materials letters* **2014**, *131*, 16-18.
47. Selvarajan, E.; Mohanasrinivasan, V. Biosynthesis and characterization of ZnO NPs using Lactobacillus plantarum VITES07. *Materials Letters* **2013**, *112*, 180-182.
48. Jayappa, M.D.; Ramaiah, C.K.; Kumar, M.A.P.; Suresh, D.; Prabhu, A.; Devasya, R.P.; Sheikh, S. Green synthesis of zinc oxide NPs from the leaf, stem and in vitro grown callus of Mussaenda frondosa L.: characterization and their applications. *Applied nanoscience* **2020**, *10*, 3057-3074.
49. Karnan, T.; Selvakumar, S.A.S. Biosynthesis of ZnO NPs using rambutan (Nephelium lappaceumL.) peel extract and their photocatalytic activity on methyl orange dye. *Journal of molecular Structure* **2016**, *1125*, 358-365.
50. Jeevanandam, J.; Barhoum, A.; Chan, Y.S.; Dufresne, A.; Danquah, M.K. Review on NPs and nanostructured materials: history, sources, toxicity and regulations. *Beilstein journal of nanotechnology* **2018**, *9*, 1050-1074.
51. Gautam, S.K.; Sapkota, B.; Bhujel, A.; Bhattarai, S. Estimation of Particle Size and Band Gap of Zinc Oxide Nanoparticle Synthesized by Chemical Precipitation Method. *Journal of Nepal Chemical Society* **2020**, *41*, 46-50.
52. Rai, A.; Singh, A.; Ahmad, A.; Sastry, M. Role of halide ions and temperature on the morphology of biologically synthesized gold nanotriangles. *Langmuir* **2006**, *22*, 736-741.

53. Das, A.K.; Marwal, A.; Verma, R. Bio-reductive synthesis and characterization of plant protein coated magnetite NPs. *Nano Hybrids and Composites* **2014**, *7*, 69.
54. Moldovan, B.; Sincari, V.; Perde-Schrepler, M.; David, L. Biosynthesis of silver NPs using Ligustrum ovalifolium fruits and their cytotoxic effects. *Nanomaterials* **2018**, *8*, 627.
55. Elumalai, K.; Velmurugan, S. Green synthesis, characterization and antimicrobial activities of zinc oxide NPs from the leaf extract of Azadirachta indica (L.). *Applied Surface Science* **2015**, *345*, 329-336.
56. Kavitha, M.; John, H.; Gopinath, P.; Philip, R. Synthesis of reduced graphene oxide–ZnO hybrid with enhanced optical limiting properties. *Journal of Materials Chemistry C* **2013**, *1*, 3669-3676.
57. Awwad, A.M.; Amer, M.W.; Salem, N.M.; Abdeen, A.O. Green synthesis of zinc oxide NPs (ZnO-NPs) using Ailanthus altissima fruit extracts and antibacterial activity. *Chem. Int* **2020**, *6*, 151-159.
58. Yusof, H.M.; Mohamad, R.; Zaidan, U.H.; Samsudin, A.A. Biosynthesis of zinc oxide NPs by cell-biomass and supernatant of Lactobacillus plantarum TA4 and its antibacterial and biocompatibility properties. *Scientific Reports* **2020**, *10*, 1-13.
59. Markus, J.; Mathiyalagan, R.; Kim, Y.-J.; Abbai, R.; Singh, P.; Ahn, S.; Perez, Z.E.J.; Hurh, J.; Yang, D.C. Intracellular synthesis of gold NPs with antioxidant activity by probiotic Lactobacillus kimchicus DCY51T isolated from Korean kimchi. *Enzyme and microbial technology* **2016**, *95*, 85-93.
60. Degen, A.; Kosec, M. Effect of pH and impurities on the surface charge of zinc oxide in aqueous solution. *Journal of the European Ceramic Society* **2000**, *20*, 667-673.
61. An, C.; Peng, S.; Sun, Y. Facile synthesis of sunlight-driven AgCl: Ag plasmonic nanophotocatalyst. *Advanced Materials* **2010**, *22*, 2570-2574.
62. Suwanchawalit, C.; Wongnawa, S. Influence of calcination on the microstructures and photocatalytic activity of potassium oxalate-doped TiO2 powders. *Applied Catalysis A: General* **2008**, *338*, 87-99.
63. Castillo, N.C.; Heel, A.; Graule, T.; Pulgarin, C. Flame-assisted synthesis of nanoscale, amorphous and crystalline, spherical BiVO4 with visible-light photocatalytic activity. *Applied Catalysis B: Environmental* **2010**, *95*, 335-347.
64. Li, F.-t.; Zhao, Y.; Liu, Y.; Hao, Y.-j.; Liu, R.-h.; Zhao, D.-s. Solution combustion synthesis and visible light-induced photocatalytic activity of mixed amorphous and crystalline MgAl2O4 nanopowders. *Chemical Engineering Journal* **2011**, *173*, 750-759.

 doi:10.20944/preprints202104.0038.v1

65. Wang, F.; Min, S.; Han, Y.; Feng, L. Visible-light-induced photocatalytic degradation of methylene blue with polyaniline-sensitized TiO2 composite photocatalysts. *Superlattices and Microstructures* **2010**, *48*, 170-180.
66. Li, X.; Liu, G.; Zhao, J. Two competitive primary processes in the photodegradation of cationic triarylmethane dyes under visible irradiation in TiO2 dispersions. *New Journal of Chemistry* **1999**, *23*, 1193-1196.
67. Lachheb, H.; Puzenat, E.; Houas, A.; Ksibi, M.; Elaloui, E.; Guillard, C.; Herrmann, J.-M. Photocatalytic degradation of various types of dyes (Alizarin S, Crocein Orange G, Methyl Red, Congo Red, Methylene Blue) in water by UV-irradiated titania. *Applied Catalysis B: Environmental* **2002**, *39*, 75-90.
68. Hu, C.; Jimmy, C.Y.; Hao, Z.; Wong, P.K. Photocatalytic degradation of triazine-containing azo dyes in aqueous TiO2 suspensions. *Applied Catalysis B: Environmental* **2003**, *42*, 47-55.
69. Eskizeybek, V.; Sarı, F.; Gülce, H.; Gülce, A.; Avcı, A. Preparation of the new polyaniline/ZnO nanocomposite and its photocatalytic activity for degradation of methylene blue and malachite green dyes under UV and natural sun lights irradiations. *Applied Catalysis B: Environmental* **2012**, *119*, 197-206.
70. Kitture, R.; Koppikar, S.J.; Kaul-Ghanekar, R.; Kale, S. Catalyst efficiency, photostability and reusability study of ZnO NPs in visible light for dye degradation. *Journal of physics and chemistry of solids* **2011**, *72*, 60-66.